

This document is confidential and is proprietary to the American Chemical Society and its authors. Do not copy or disclose without written permission. If you have received this item in error, notify the sender and delete all copies.

## Hyperbranched Quasi-1D TiO<sub>2</sub> Nanostructure for Hybrid Organic-Inorganic Solar Cells

Journal:	<i>ACS Applied Materials &amp; Interfaces</i>
Manuscript ID:	am-2014-090429.R2
Manuscript Type:	Letter
Date Submitted by the Author:	24-Mar-2015
Complete List of Authors:	Ghadirzadeh, Ali; Center for Nanoscience and Technology @PoliMi, Istituto Italiano di Tecnologia Passoni, Luca; Istituto Italiano di Tecnologia - Center For Nano Science and Technology, Grancini, Giulia; IIT Italian Institute of Technology - CNST@PoliMi, Terraneo, Giancarlo; Politecnico di Milano, Laboratory of Nanostructured Fluorinated Materials Li Bassi, Andrea; Politecnico di Milano, Department of Energy Petrozza, Annamaria; Italian Institute of Technology, Center for Nano Science and Technology Di Fonzo, Fabio; Istituto Italiano di Tecnologia, Center for Nanoscience and Technology

SCHOLARONE™  
Manuscripts

# Hyperbranched Quasi-1D TiO<sub>2</sub> Nanostructure for Hybrid Organic-Inorganic Solar Cells

Ali Ghadirzadeh,<sup>a,b</sup> Luca Passoni,<sup>a,c</sup> Giulia Grancini,<sup>a</sup> Giancarlo Terraneo,<sup>d</sup> Andrea Li Bassi,<sup>a,b</sup>  
Annamaria Petrozza,<sup>a</sup> Fabio Di Fonzo<sup>a\*</sup>

<sup>a</sup> Center for Nanoscience and Technology @PoliMi, Istituto Italiano di Tecnologia, Via Pascoli 70/3, 20133 Milano, Italy

<sup>b</sup> Politecnico di Milano, Dip.to di Energia, Via Ponzio, 20133 Milano, Italy

<sup>c</sup> Politecnico di Milano, Dip.to di Fisica, P.zza L. Da Vinci 32, 20133 Milano, Italy

<sup>d</sup> Laboratory of Nanostructured Fluorinated Materials (NFMLab), Department of Chemistry, Materials, and Chemical Engineering “Giulio Natta”, Politecnico di Milano, Milan, Italy

**KEYWORDS** Hyperbranched nanostructures, hybrid solar cells, pulsed laser deposition, P3HT, 1D nanostructures, self-assembled

## ABSTRACT

The performance of hybrid solar cells is strongly affected by the device morphology. In this work we demonstrate a Poly(3-hexylthiophene-2,5-diyl)/TiO<sub>2</sub> hybrid solar cell where the TiO<sub>2</sub> photoanode comprises an array of tree-like hyperbranched quasi-1D nanostructures self-assembled from the gas phase. This advanced architecture enables us to increase the power conversion efficiency to over 1%, doubling the efficiency with respect to state of the art devices employing standard mesoporous titania photoanodes. This improvement is attributed to several peculiar features of this array of nanostructures: high interfacial area; increased optical density thanks to the enhanced light scattering; and enhanced crystallization of Poly(3-hexylthiophene-2,5-diyl) inside the quasi-1D nanostructure.

1 Hybrid solar energy devices (HSC) comprise a high band-gap n-type metal oxide nanostructure, commonly  
2 TiO<sub>2</sub>, and a light absorbing conjugated polymer functioning as hole-transporting material.<sup>1-3</sup> Upon light  
3 illumination, photo-induced excitons are generated in the organic material and charge separation takes place at  
4 the organic-inorganic interface where electrons are injected into the inorganic semiconductor.<sup>4,5</sup> The  
5 morphology of the active layer strongly affects the performance of hybrid devices, thus proper engineering of  
6 the organic-inorganic heterojunction remains a key issue in developing hybrid solar cells.<sup>6-8</sup> The key features for  
7 an efficient device are: (i) high interfacial area between the acceptor and the donor materials in order to increase  
8 the active area for charge separation; (ii) continuous pathways for the separated charges in order for them to  
9 reach the electrodes and avoid recombination in lattice traps and defects; (iii) organic domains with dimensions  
10 not exceeding in size the exciton diffusion length which is in the order of 5-20 nm. The most common  
11 approach<sup>9,10</sup> consists in blending inorganic nanocrystals with an organic conjugated polymer. Despite this  
12 simple method, which achieves a high interfacial area, it presents issues related to blend inhomogeneity and  
13 instability of the mixture, which over time leads to a disordered matrix with little control over the polymer  
14 domain size. While efficient charge separation is eased by a large interfacial area, exciton migration to the  
15 interface is hampered by large polymer domains and charge collection is prevented by the random blend  
16 network. HSC based on the TiO<sub>2</sub>/Poly(3-hexylthiophene-2,5-diyl) (*i.e.* TiO<sub>2</sub>/P3HT) blend have not been able to  
17 reach a power conversion efficiency higher than 0.5%.<sup>11</sup> An alternative solution is to use one dimensional  
18 nanostructures such as nanowires<sup>12</sup> or nanotubes<sup>13</sup> that provide preferential carrier pathways, thus reducing  
19 charge recombination.<sup>14,15</sup> A further advantage of 1D structures is the potential for increasing polymer  
20 crystallinity by enhancing alignment of P3HT chains along their structures. As demonstrated by K.M Coakley *et*  
21 *al.*, a 20 fold increase in hole mobility can be achieved in crystallized P3HT molecules infiltrated in ordered  
22 nanotubes.<sup>16</sup> A power conversion efficiency of close to 1% has been achieved,<sup>17</sup> but the modest specific surface  
23 area has kept this approach far away from the ideal structure. An different approach to induce ordering of the  
24 polymer at the interface with TiO<sub>2</sub> is the use of molecular interlayers, as reported by some of the co-authors of  
25 this work<sup>18</sup> increasing power conversion efficiency from 0.37% to 0.95%. While a comparative table is  
26 provided in the Supporting Information, a complete review on the performances of different hybrid devices can  
27 be found in the literature.<sup>19</sup>

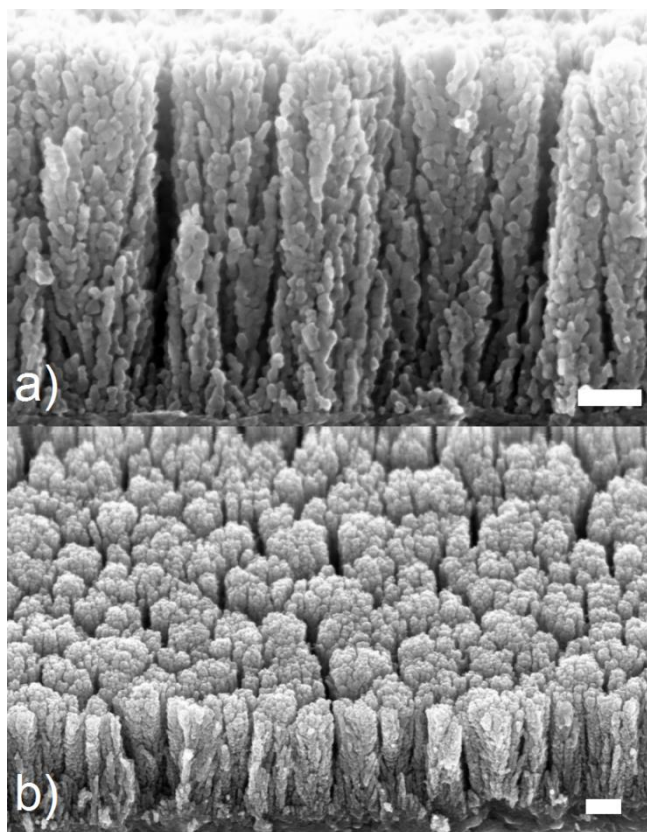


**Figure 1.** Crystalline hyperbranched TiO<sub>2</sub> deposited at 7 Pa Oxygen pressure; a) cross-sectional view; b) tilted view showing both cross-section and top surface of the hyperbranched nanostructures. Scale bar: 100 nm.

In our previous work,<sup>20</sup> hierarchical TiO<sub>2</sub> nanostructures were modelled by high-angle annular dark field scanning transmission electron microscopy (HAADF-STEM) tomography to gain insight into their 3D structure. Monotonic connectivity, defined as the ratio of the titanium dioxide in contact with the electrodes through a decreasing path length, was found to be 0.89 when considering the bottom electrode *versus* 0.69 when considering the top contact. Such geometrical asymmetry in the titanium dioxide structures is thought to favour electron transport toward the anode, reducing the recombination rate of photo-generated charges. Geometrical tortuosity of the hierarchical structure, defined as the ratio between the length of the shortest charge collection path divided by the orthogonal distance along the z-axis, was also analysed. The average values were found to be 1.466 and 1.559 toward the anode and in the opposite direction respectively (comparable to literature values ranging from 1.0 to 2.0).<sup>21,22</sup> These values are also the evidence that the directional morphology of these structures is facilitating electron transport toward the anode. Further analysis in the presence of infiltrated P3HT showed that over 75% of the polymer volume is within 8.5 nm of the interface crucial for a high rate of exciton

1 collection. A prototype non-optimized hybrid solar cell with an efficiency of 0.66% was reported as an example.  
2  
3 The optimization of the pulsed laser deposition allowed for the fabrication of a complex film morphology  
4 comprising an array of quasi-1D hyperbranched nanostructures with high specific surface area and directional  
5 porosity along the film thickness. This nano-architecture, previously shown to work as an efficient photoanode  
6 in liquid and solid DSSC,<sup>23,24</sup> indeed presents an interconnected network with open channels and high specific  
7 surface area. Quasi-1D hyperbranched nanostructures, thanks to their size being in the range of the wavelength  
8 of visible light, act as integrated Mie scattering elements diffusing the transmitted light and enhancing the  
9 device optical thickness eventually improving light absorption and photogenerated current (as reported in other  
10 works).<sup>25</sup> For the fabrication of such nanostructures, pulsed laser deposition is performed inside a vacuum  
11 chamber in presence of a background gas. In a certain range of deposition parameters multidirectional cluster  
12 scattering is induced so that an array of quasi-1D hierarchical nanostructures grows directly from the gas phase  
13 perpendicular to the substrate. The film thickness is a function of laser energy and increases linearly with  
14 deposition time. The film porosity, specific surface area and pore diameter characteristics of the nanostructures  
15 are a function of the deposition pressure and annealing temperature. The as deposited films are amorphous and  
16 are typically annealed at 500°C for 2 hours in air to achieve the anatase crystalline phase. This allotropic phase  
17 is well known to optimize charge injection and transport as well as the maximal specific surface area  
18 requirements. As reported in previous publications, film possessing at a given density, upon thermal treatment,  
19 shows preferential crystal growth along the [004] direction forming hyperbranched nanostructures, sometimes  
20 referred to as nanotrees.<sup>24, 26</sup> Through TEM and X-Ray diffraction analysis it was demonstrated that among the  
21 annealed samples deposited at different pressures, those deposited at an O<sub>2</sub> pressure of 7 Pa were optimal for  
22 obtaining a hyperbranched structure with a crystal domain size of several tens of nanometers along the *c*  
23 direction [004].<sup>24</sup> An example of the hyperbranched assembly is presented in Figure 1. Here we show how  
24 optimized quasi-1D hyperbranched nanostructure self-assembled from the gas phase by PLD (deposited in 7 Pa  
25 of O<sub>2</sub>) enhances the photovoltaic performance in hybrid organic solar cells when compared to standard  
26 mesoporous/P3HT devices (see methods in Supporting Information for details on material and device  
27 fabrication and characterization). In order to be consistent with the above mentioned published work,<sup>18</sup> we used  
28 the optimized reference architecture found there as a benchmark throughout this study. In HSCs, the  
29 morphology of the nanostructured photoanode must comprise pores sufficiently large and interconnected to  
30 allow continuous polymer infiltration and, at the same time, polymer domains smaller than the exciton diffusion  
31  
32  
33  
34  
35  
36  
37  
38  
39  
40  
41  
42  
43  
44  
45  
46  
47  
48  
49  
50  
51  
52  
53  
54  
55  
56  
57  
58  
59  
60

length to impede exciton recombination. Using Brunauer-Emmett-Teller (BET) technique, it was shown that a low deposition pressure resulted in a low porosity (high density) and low specific surface area film, while a high deposition pressure resulted in a high porosity (low density) and high specific surface area.<sup>24</sup> It should be noted that for a photoanode composed of hyperbranched structures, the polymer must infiltrate into a complex hierarchical void path. While nanometric voids (spaces between braches) fulfil the dimensional requirements imposed by the exciton diffusion length, in the case of films with excessive porosity the micrometric channels among 1D hyperbranched nanostructures are thought to be responsible for polymer accumulation in domains big enough (>50 nm) to hamper exciton diffusion and thus charge separation.<sup>27</sup> In Figure S1 in the Supporting Information, the optical transmittance for the films with different porosities infiltrated with P3HT is reported to demonstrate that a larger amount of infiltrated polymer is present in the more porous structures (*i.e.* lower transmittance). The effect of film thickness is investigated on films ranging from 0.1 to 2  $\mu\text{m}$  showing the best results for an 800 nm thick film (Figure S2) and it is compared to the average and maximum performance of control devices comprising a nanoparticle-based photoanode., fabricated following the protocol reported in previous work.<sup>18</sup> The number of charge recombination sites is increased in thinner film by polymer accumulation and in the case of thicker films by the excessive length of the electron path. Indeed, the series resistance is found to be minimized for 800 nm thick samples deposited at 7 Pa, while increases for both thinner and thicker devices can be seen in Figure S3 in the electronic Supporting Information.

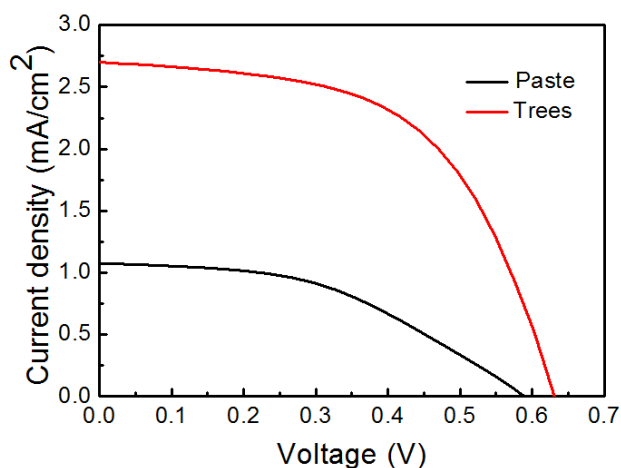
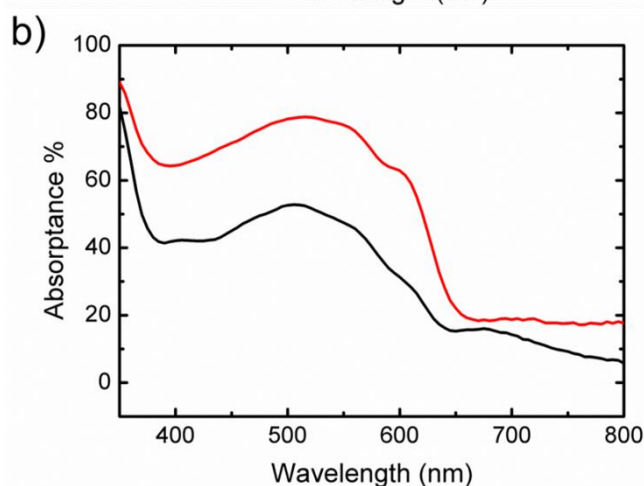
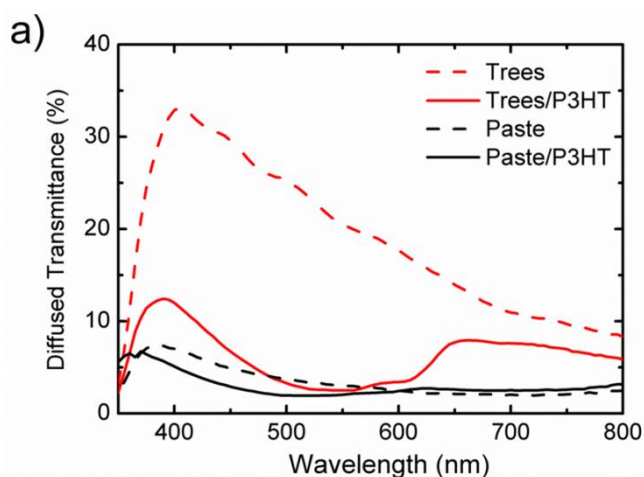


**Figure 2.** Performance comparison between devices comprising hyperbranched photoanode and standard mesoporous photoanode.

1  
2 For devices based on the hyperbranched photoanode (h-PA) an average power conversion efficiency of 0.8%,  
3 exceeding 1% for the best device, is recorded. Performance of the optimized h-PA devices, are compared with a  
4 standard mesoporous structure prepared using a titanium dioxide nanoparticle paste mixed with the same  
5 polymer. The J-V curves of champion devices can be found in Figure 2 where a greater than 2 fold increase in  
6 performance (PCE=1% and PCE=0.34% for the h-PA device and the standard device respectively) mainly due  
7 to the enhancement in photo-generated current ( $2.7 \text{ mA/cm}^2$  and  $1.15 \text{ mA/cm}^2$  for the h-PA device and the  
8 standard device respectively) is reported. This 130% current density improvement is in the first instance  
9 attributed to light scattering in the hyperbranched nanostructure increasing the device optical thickness and  
10 enhancing its light-harvesting efficiency. The optical characterization of the devices was performed both on  
11 crystalline mesoporous and hyperbranched optimized photoanodes before and after P3HT infiltration. Figure S4  
12 shows a schematic illustration of the comparison between the mesoporous structure (a) and the hierarchical  
13 nanostructure (b).

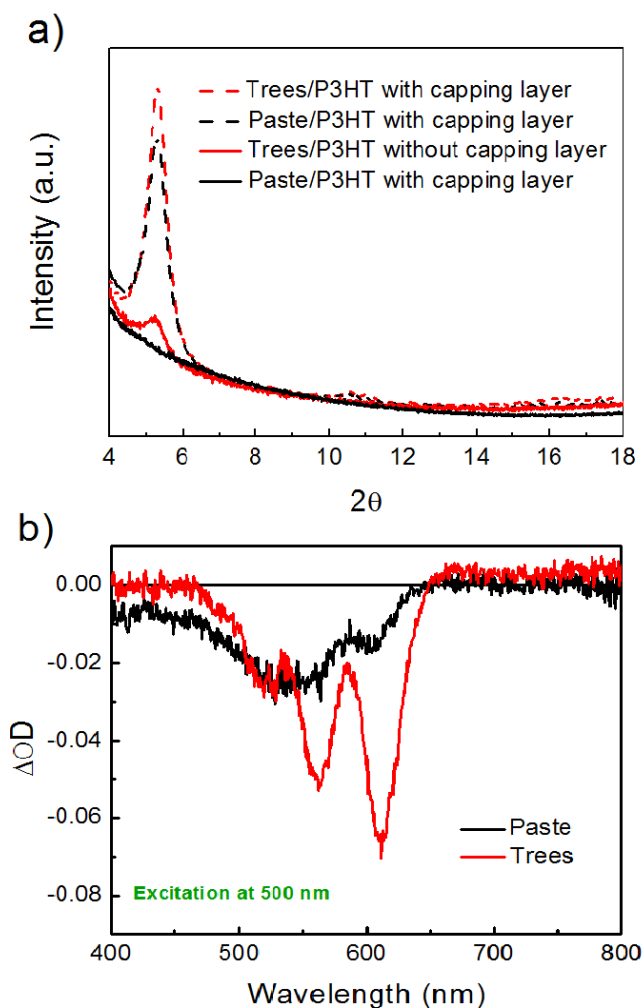


1  
2 **Figure 3.** Optical characterization curves for the optimized h-PA device (red) in comparison to standard  
3 mesoporous structure (black): a) diffused transmittance b) absorptance of TiO<sub>2</sub>/P3HT.  
4  
5  
6

7 While the total transmittance and the haze factor can be found in electronic Supporting Information (Figure S5),  
8  
9 Figures 3a shows the diffuse transmittance curves for both structures, with and without P3HT. The  
10 hyperbranched photoanode, in comparison to the one with standard nanoparticles, shows significantly higher  
11 diffuse transmittance indicating higher light scattering. This behaviour can be explained by the fact that h-PAs  
12 are composed of arrays of nanotrees with a characteristic longitudinal size of the same order of magnitude as the  
13 incident light. Acting as scattering elements, these structures enhance the photoanode optical thickness,  
14 increasing the photon interaction with the photoactive layer therefore enhancing the PCE. As can be seen in  
15 Figure 3a, scattering increases in the spectral range around 450 nm, which is the wavelength for which the  
16 characteristic size of quasi 1D hyperbranched nanostructure presents a higher scattering cross-section. In Figure  
17 3b absorptance curves are presented showing an increase of optical density for a hyperbranched structure when  
18 compared to standard mesoporous nanoparticles. Over the visible range an average absorptance increase of  
19 +60% in the h-PA devices can be observed in comparison with a standard nanoparticle-based device. The  
20 absorbance curve of P3HT over the hyperbranched nanostructure differs from that of the mesoporous paste. If  
21 normalized (Figure S6), it becomes evident that for the h-PA device an increase in the 380-430 nm range arises  
22 as a consequence of the strong scattering that characterizes this spectral region. Interestingly, a higher relative  
23 intensity for wavelengths around 630 nm is also observed. The latter phenomenon could be ascribed to a more  
24 intense vibronic structure resulting from a higher molecular order in the polymer<sup>28,29</sup> when infiltrated into the  
25 quasi 1D nanostructure rather than into the mesoporous film. In order to further study the effect of the inorganic  
26 scaffold on polymer crystallinity, X-ray diffraction is used and results are reported in Figure 4a. The analysis  
27 has been performed on scaffolds with and without the polymer capping layer (SEM images of the cross sections  
28 of these samples are reported in Figure S7 in the Supporting Information). In the presence of a capping layer the  
29 strong peak at  $2\theta = 5.4^\circ$ , related to the (100) plane of crystalline P3HT, is present despite the nature of the  
30 scaffold. On the other hand, when the polymer is only present in the oxide scaffold, only the 1D hyperbranched  
31 structures show crystalline phases. To relate this structural information to the operation of the solar cell we have  
32 performed time-resolved pump probe on a time window of hundreds of nanoseconds, when long living charge  
33 carriers represent the main photo-excited population. Differential Absorption spectra integrated in the first 500  
34 ns upon excitation at 500 nm for the P3HT/Trees (red) and P3HT/Paste (black) samples are displayed in Figure  
35  
36  
37  
38  
39  
40  
41  
42  
43  
44  
45  
46  
47  
48  
49  
50  
51  
52  
53  
54  
55  
56  
57  
58  
59  
60



4b. The spectra reveal a negative signal in the 450-620 nm region that is due to P3HT photobleaching (PB) in good agreement with the absorption spectrum. The PB band at this timescale is related to charges. The polymer deposited on the h-PA photoanode shows a much more resolved structure of the photobleaching with a high relative intensity of the vibronic peaks.<sup>30</sup> On the other hand, the P3HT infiltrated into TiO<sub>2</sub> paste shows a blue-shifted absorption and a less pronounced vibronic structure. As it is well known that these optical features are correlated to specific morphological characteristics of the conjugated polymer - i.e. to crystalline phases in the first case, disordered/amorphous phases in the latter- we can conclude that in presence of 1-D hyperbranched nanostructures, photocarriers are mainly moving along ordered crystalline structures that can sustain higher carrier mobility and lower recombination processes at the interface.<sup>30,31</sup> Moreover, considering that in a complete device structure the polymer capping layer over the scaffold tends to reach a higher level of order (thus a smaller band-gap), independently of the nature of the layer underneath, the possibility of also achieving a long range order in the bulk reduces the degree of energetic disorder in the device which would affect the harvesting of photogenerated excitons away from the interface and the collection of carriers.



1  
2 **Figure 4.** Evidence for P3HT crystallinity. Hyperbranched structures (red) and mesoporous nanoparticle paste  
3 (black) a) XRD spectra of the films with P3HT capping layer (dashed line) and without P3HT capping layer  
4 (solid line) and b) nanosecond transient absorption.  
5  
6  
7  
8

9 In this work, we demonstrated the fabrication of a quasi-1 D hyperbranched nanostructure of TiO<sub>2</sub>, self-  
10 assembled from the gas phase by means of pulsed laser deposition and its successful application as a  
11 photoanode in hybrid organic-inorganic solar cells. Self-assembled quasi 1D hyperbranched nanostructures were  
12 coupled with P3HT in a hybrid solar cell. A power conversion efficiency of 1% was achieved. Such a result  
13 originates from an increase in photogenerated current as a consequence of the higher optical thickness of h-PA  
14 devices induced by strong light scattering. Moreover, devices comprising quasi 1D hyperbranched  
15 nanostructures could also benefit from fast electron transport, high interfacial area between the polymeric and  
16 inorganic phases, and from P3HT molecular ordering.  
17  
18  
19  
20  
21  
22  
23  
24  
25  
26  
27  
28  
29  
30  
31  
32  
33  
34  
35  
36  
37  
38  
39  
40  
41  
42  
43  
44  
45  
46  
47  
48  
49  
50  
51  
52  
53  
54  
55  
56  
57  
58  
59  
60

1  
2 ASSOCIATED CONTENT  
3  
4

5 Total transmittance of film at different porosity, device thickness optimization, devices series resistance, optical  
6 analysis, SEM cross-section of P3HT infiltrated films. This material is available free of charge via the Internet  
7 at <http://pubs.acs.org>.  
8  
9

10  
11 AUTHOR INFORMATION  
1213  
14 **Corresponding Author**  
15

16 \* Fabio Di Fonzo. Email: [fabio.difonzo@iit.it](mailto:fabio.difonzo@iit.it) Tel. +39 0223999868  
17  
18

19  
20 ACKNOWLEDGMENT  
21

22 We would like to acknowledge James Ball for helping in revising the manuscript.  
23  
24  
25  
26  
27

28 REFERENCES  
29

- 30 (1) Weickert, J.; Auras, F.; Bein, T.; Schmidt-Mende, L. Characterization of Interfacial Modifiers for  
31 Hybrid Solar Cells. *J. Phys. Chem. C* **2011**, *115*, 15081–15088.  
32  
33 (2) Boucle, J.; Ravirajan, P.; Nelson, J. Hybrid Polymer–Metal Oxide Thin Films for Photovoltaic  
34 Applications. *J. Mater. Chem.* **2007**, *17*, 3141-3153.  
35  
36 (3) Zhang, G.; Finefrock, S.; Liang, D.; Yadav, G. G.; Yang, H.; Fang, H.; Wu, Y. Semiconductor  
37 Nanostructure-Based Photovoltaic Solar Cells. *Nanoscale* **2011**, *3*, 2430-2443.  
38  
39 (4) Weickert, J.; Dunbar, R. B.; Hesse, H. C.; Wiedemann, W.; Schmidt-Mende, L. Nanostructured Organic  
40 and Hybrid Solar Cells. *Adv. Mater.* **2011**, *23*, 1810-1828.  
41  
42 (5) Zhou, R.; Xue, J. Hybrid Polymer-Nanocrystal Materials for Photovoltaic Applications.  
43 *ChemPhysChem* **2012**, *13*, 2471-2480.  
44  
45 (6) Chen, W.; Nikiforov, M. P.; Darling, S. B. Morphology Characterization in Organic and Hybrid Solar  
46 Cells. *Energy Environ. Sci.* **2012**, *5*, 8045-8074  
47  
48 (7) Gur, I.; Fromer, N. A.; Chen, C.-P.; Kanaras, A. G.; Alivisatos, A. P. Hybrid Solar Cells with  
49 Prescribed Nanoscale Morphologies Based on Hyperbranched Semiconductor Nanocrystals. *Nano Lett.* **2007**, *7*,  
50 409-414.  
51  
52  
53  
54  
55  
56  
57  
58  
59  
60

- 1  
2 (8) Iza, D.; Muñoz-Rojas, D.; Musselman, K.; Weickert, J.; Jakowetz, A.; Sun, H.; Ren, X.; Hoye, R.; Lee,  
3 J.; Wang, H. *et al.* Nanostructured Conformal Hybrid Solar Cells: a Promising Architecture Towards Complete  
4 Charge Collection and Light Absorption. *Nanoscale Res. Lett.* **2013**, *8*, 1-9.  
5  
6  
7  
8 (9) Wright, M.; Uddin, A. Organic-Inorganic Hybrid Solar Cells: A Comparative Review. *Sol. Energy*  
9 *Mater. Sol. Cells* **2012**, *107*, 87-111.  
10  
11  
12 (10) Chandrasekaran, J.; Nithyaprakash, D.; Ajjan, K. B.; Maruthamuthu, S.; Manoharan, D.; Kumar, S.  
13 Hybrid Solar Cell Based on Blending of Organic and Inorganic Materials-an Overview. *Renewable Sustainable*  
14 *Energy Rev.* **2011**, *15*, 1228-1238.  
15  
16  
17 (11) Coakley, K. M.; McGehee, M. D. Photovoltaic Cells Made from Conjugated Polymers Infiltrated into  
18 Mesoporous Titania. *Appl. Phys. Lett.* **2003**, *83*, 3380-3382.  
19  
20  
21 (12) Zhang, Q.; Yodyingyong, S.; Xi, J.; Myers, D.; Cao, G. Oxide Nanowires for Solar Cell Applications.  
22 *Nanoscale* **2012**, *4*, 1436-1445.  
23  
24  
25 (13) Wisnet, A.; Thomann, M.; Weickert, J.; Schmidt-Mende, L.; Scheu, C. Nanoscale Investigation on  
26 Large Crystallites in TiO<sub>2</sub> Nanotube Arrays and Implications for High-Quality Hybrid Photodiodes. *J. Mater.*  
27 *Sci.* **2012**, *47*, 6459-6466.  
28  
29  
30 (14) Yu, K.; Chen, J. Enhancing Solar Cell Efficiencies Through 1-D Nanostructures. *Nanoscale Res. Lett.*  
31 **2009**, *4*, 1-10.  
32  
33  
34 (15) Sato, K.; Dutta, M.; Fukata, N. Inorganic/Organic Hybrid Solar Cells: Optimal Carrier Transport in  
35 Vertically Aligned Silicon Nanowire Arrays. *Nanoscale* **2014**, *6*, 6092-6101.  
36  
37  
38 (16) Coakley, K. M.; Srinivasan, B. S.; Ziebarth, J. M.; Goh, C.; Liu, Y.; McGehee, M. D. Enhanced Hole  
39 Mobility in Regioregular Polythiophene Infiltrated in Straight Nanopores. *Adv. Funct. Mater.* **2005**, *15*, 1927-  
40 1932.  
41  
42  
43 (17) Wu, M. C.; Chang, C. H.; Lo a, H. H.; Lin, Y. S.; Lin, Y. Y.; Yen, W. C.; Su, W. F.; Chen, Y. F.; Chen,  
44 C. W. Nanoscale Morphology and Performance of Molecular-Weight-Dependent Poly(3-hexylthiophene)/TiO<sub>2</sub>  
45 Nanorod Hybrid Solar Cells. *J. Mater. Chem.* **2008**, *18*, 4097-4102.  
46  
47  
48 (18) Canesi, E. V.; Binda, M.; Abate, A.; Guarnera, S.; Moretti, L.; D'Innocenzo, V.; Sai Santosh Kumar, R.;  
49 Bertarelli, C.; Abrusci, A.; Snaith, H.; *et al.* The Effect Of Selective Interactions at the Interface of Polymer-  
50 Oxide Hybrid Solar Cells. *Energy Environ. Sci.* **2012**, *5*, 9068-9076.  
51  
52  
53  
54  
55  
56  
57  
58  
59  
60

- 1  
2 (19) Wright, M.; Uddin, A. Organic—Inorganic Hybrid Solar Cells: a Comparative Review. *Sol. Energy*  
3 *Mater. Sol. Cells* **2012**, *107*, 87-111.
- 4  
5 (20) Divitini, G.; Stenzel, O.; Ghadirzadeh, A.; Guarnera, S.; Russo, V.; Casari, C. S.; Bassi, A. L.; Petrozza,  
6 A.; Di Fonzo, F.; Schmidt, V.; *et al.* Nanoscale Analysis of a Hierarchical Hybrid Solar Cell in 3D. *Adv. Funct.*  
7 *Mater.* **2014**, *24*, 3043-3050.
- 8  
9 (21) Kroese, D. P.; Brereton, T.; Taimre, T.; Botev, Z. I. Why the Monte Carlo Method is so Important  
10 Today. *Comput. Stat.* **2014**, *6*, 386-392.
- 11  
12 (22) Thiedmann, R.; Stenzel, O.; Spettl, A.; Shearing, P. R.; Harris, S. J.; Brandon, N. P.; Schmidt, V.  
13 Stochastic Simulation Model for the 3D Morphology of Composite Materials in Li-ion Batteries. *Comput.*  
14 *Mater. Sci.* **2011**, *50*, 3365-3376.
- 15  
16 (23) Sauvage, F.; Di Fonzo, F.; Li Bassi, A.; Casari, C. S.; Russo, V.; Divitini, G.; Ducati, C.; Bottani, C. E.;  
17 Comte, P.; Graetzel, M. Hierarchical TiO<sub>2</sub> Photoanode for Dye-Sensitized Solar Cells. *Nano Lett.* **2010**, *10*,  
18 2562-2567.
- 19  
20 (24) Passoni, L.; Ghods, F.; Docampo, P.; Abrusci, A.; Martí-Rujas, J.; Ghidelli, M.; Divitini, G.; Ducati, C.;  
21 Binda, M.; Guarnera, S.; *et al.* Hyperbranched Quasi-1D Nanostructures for Solid-state Dye-sensitized Solar  
22 Cells. *ACS Nano* **2013**, *7*, 10023-10031.
- 23  
24 (25) Lin, J.; Heo, Y.-U.; Nattestad, A.; Yamauchi, Y.; Dou, S. X.; Kim, J. H., Mesoporous Hierarchical  
25 Anatase for Dye-sensitized Solar Cells Achieving Over 10% Conversion Efficiency. *Electrochim. Acta* **2015**,  
26 *153*, 393-398.
- 27  
28 (26) Jun, Y.; Casula, M. F.; Sim, J.; Kim, S. Y.; Cheon, J.; Alivisatos, A. P. Surfactant-Assisted Elimination  
29 of a High Energy Facet as a Means of Controlling the Shapes of TiO<sub>2</sub> Nanocrystals. *J. Am. Chem. Soc.* **2003**,  
30 *125*, 15981-15985.
- 31  
32 (27) Divitini, G.; Abrusci, A.; Fonzo, F. D.; Snaith, H.; Ducati, C. Quantitative Electron Tomography  
33 Investigation of a TiO<sub>2</sub> Based Solar Cell Photoanode. *J. Phys.: Conf. Ser.* **2014**, *522*, 012063.
- 34  
35 (28) Hintz, H.; Egelhaaf, H. J.; Luer, L.; Hauch, J.; Peisert, H.; Chasse, T. Photodegradation of P3HT-a  
36 Systematic Study of Environmental Factors. *Chem. Mater.* **2011**, *23*, 145-154.
- 37  
38 (29) Brown P. J.; Thomas, D. S.; Köhler, A.; Wilson, J. S.; Kim, J.; Ramsdale, C. M.; Siringhaus, H.;  
39 Friend, R. H. Effect of Interchain Interactions on the Absorption and Emission of Poly(3-hexylthiophene). *Phys.*  
40 *Rev. B* **2003**, *67*, 064203.
- 41  
42  
43  
44  
45  
46  
47  
48  
49  
50  
51  
52  
53  
54  
55  
56  
57  
58  
59  
60

1  
2 (30) Guo, J.; Ohkita, H.; Bente, H.; Ito, S. Charge Generation and Recombination Dynamics in Poly(3  
3 hexylthiophene)/Fullerene Blend Films with Different Regioregularities and Morphologies. *J. Am. Chem. Soc.*  
4 **2010**, *132*, 6154–6164.  
5  
6

7  
8 (31) Guo, J.; Ohkita, H.; Bente, H.; Ito, S. Near-IR Femtosecond Transient Absorption Spectroscopy of  
9 Ultrafast Polaron and Triplet Exciton Formation in Polythiophene Films with Different Regioregularities. *J. Am.*  
10 *Chem. Soc.* **2009**, *131*, 16869–16880.  
11  
12  
13  
14  
15  
16  
17

